Supporting Information

On-surface synthesis and characterization of Teranthene and Hexanthene: Ultrashort graphene nanoribbons with mixed armchair and zigzag edges

Gabriela Borin Barin[1]*, Marco Di Giovannantonio[1]*[+], Thorsten G. Lohr[2]*, Shantanu Mishra[1++], Amogh Kinikar[1], Mickael L. Perrin[3,4], Jan Overbeck[3], Michel Calame[3,5,6], Xinliang Feng[2,7], Roman Fasel[1,8] and Pascal Ruffieux[1]

[1]nanotech@surfaces Laboratory, Empa, Swiss Federal Laboratories for Materials Science and Technology, 8600 Dübendorf, Switzerland

[2]Center for Advancing Electronics Dresden, Department of Chemistry and Food Chemistry, TU Dresden, Dresden 01062, Germany

[3]Transport at Nanoscale Interfaces Laboratory, Empa, Swiss Federal Laboratories for Materials Science and Technology, 8600 Dübendorf, Switzerland

[4]Department of Information Technology and Electrical Engineering, ETH Zurich, 8092 Zurich, Switzerland

[5]Department of Physics, University of Basel, Klingelbergstrasse 82, CH-4056 Basel, Switzerland

[6]Swiss Nanoscience Institute, University of Basel, Klingelbergstrasse 82, CH-4056 Basel, Switzerland

[7]Max Planck Institute of Microstructure Physics, Weinberg 2, 06120 Halle, Germany

[8]Department of Chemistry, Biochemistry and Pharmaceutical Sciences, University of Bern, 3012 Bern, Switzerland

[+]Present address: Istituto di Struttura della Materia – CNR (ISM-CNR), via Fosso del Cavaliere 100, Roma 00133, Italy

[++]Present address: IBM Research – Zurich, Rüschlikon 8803, Switzerland

*These authors contributed equally to this work

Precursor synthesis and characterization

Unless otherwise stated, commercially available starting materials, catalysts, reagents, and dry solvents were used without further purification. Reactions were performed using standard vacuum-line and Schlenk techniques. All the starting materials were obtained from Sigma Aldrich, or TCI. Catalysts were purchased from Strem. Column chromatography was performed on silica (SiO_2, particle size 0.063−0.200 mm, purchased from VWR). Silica-coated aluminum sheets with a fluorescence indicator (TLC silica gel 60 F_{254}, purchased from Merck KGaA) were used for thin layer chromatography.

MALDI-TOF spectra were recorded on a Bruker Autoflex Speed MALDI-TOF MS (Bruker Daltonics, Bremen, Germany). All of the samples were prepared by mixing the analyte and the matrix, 1,8-dihydroxyanthracen-9(10H)-one (dithranol, purchased from Fluka Analytical, purity >98%) in the solid state.

NMR data were recorded on a Bruker AV-II 300 spectrometer operating at 300 MHz for ^{1}H and 75 MHz for ^{13}C with standard Bruker pulse programs 333 K. Chemical shifts (δ) are reported in ppm. Coupling constants (J) are reported in Hz. Tetrachloroethane-d_2 ($\delta(^{1}H)$ = 5.91 ppm, $\delta(^{13}C)$ = 74.2 ppm) was used as solvents. The following abbreviations are used to describe peak patterns as appropriate: s = singlet, d = doublet, t = triplet, q = quartet, and m = multiplet. Tetrachloroethane-d_2 (99.9 atom% D) was purchased from Euriso-top.

Melting points were determined on a Büchi Melting Point M-560 in a range of 50−400 °C with a temperature rate of 10 °Cmin^{-1}.

10-bromo-9,9':10',9''-teranthracene (**1**)

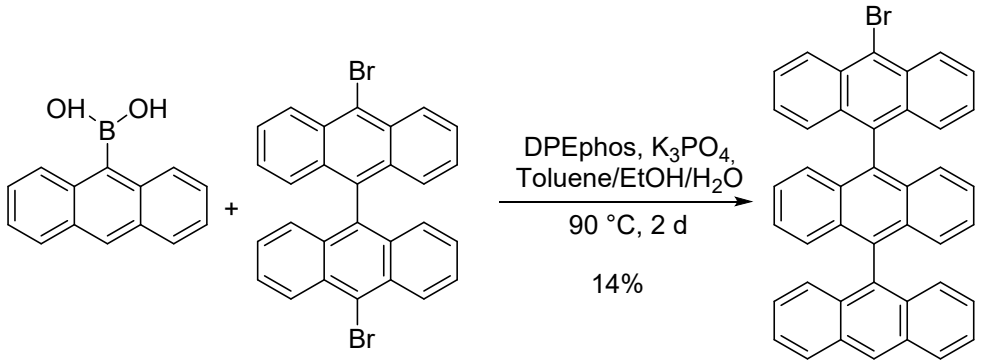

Figure S1. 10,10′-dibromo-9,9′-bianthracene (100 mg, 0,195 mmol), 9-anthraceneboronic acid (56.4 mg, 0.254 mmol, 1.3 eq.), tripotassium phosphate (207.2 mg, 0.976 mmol, 5.0 eq.), DPEphos (42 mg, 0.078 mmol, 0.4 eq.) and $Pd_2(dba)_3$ (42.1 mg, 0.078 mmol, 0.4 eq.) were added to a 50 ml schlenk flask and evacuated and refilled with argon three times. After adding the degassed solvents (5 ml toluene, 1 ml water and 0.6 ml ethanol), the reaction mixture was heated to 90 °C for 2 days. After quenching with water the product was extracted with DCM, washed with brine and dried over $MgSO_4$. The solvents were removed under vacuum. The crude material was purified by column chromatography (chloroform:isohexane = 1:5 to 1:1). After recrystallization (chloroform/MeOH) the title compound **1** was afforded in a yield of 14% (16 mg).

mp: > 400 °C; R_f: 0.30 (DCM:isohexane = 1:3); ^{1}H NMR (300 MHz, $C_2D_2Cl_4$, 333 K) δ (ppm) = 8.71 (d, J = 6.9 Hz, 3H), 8.16 (d, J = 8.5 Hz, 2H), 7.65 – 7.56 (m, 2H), 7.52 – 7.43 (m, 2H), 7.34 – 7.23 (m, 8H), 7.21 – 7.13 (m, 4H), 7.11 – 7.01 (m, 4H); ^{13}C NMR (76 MHz, $C_2D_2Cl_4$, 333K) δ (ppm) = 132.74, 131.91, 131.66, 128.97, 128.40, 127.79, 127.61, 127.30, 127.06, 126.68, 126.42, 126.00, 125.74; HR-MS (MALDI-TOF) *m/z*: [M^+] calcd for $C_{42}H_{25}Br$: 608.1130; found: 608.1128; error: -0.33 ppm.

MALDI-TOF spectra

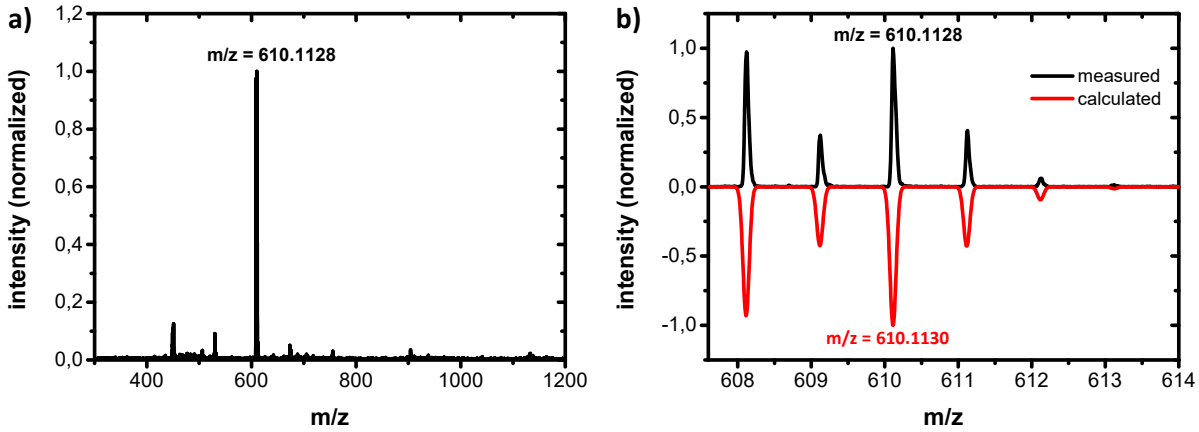

Figure S2: a) HR-MALDI-TOF spectrum of **1**; b) HR-MALDI-TOF magnified spectrum of **1** (black line) is in agreement to the expected isotopic distribution pattern (red line).

NMR spectra

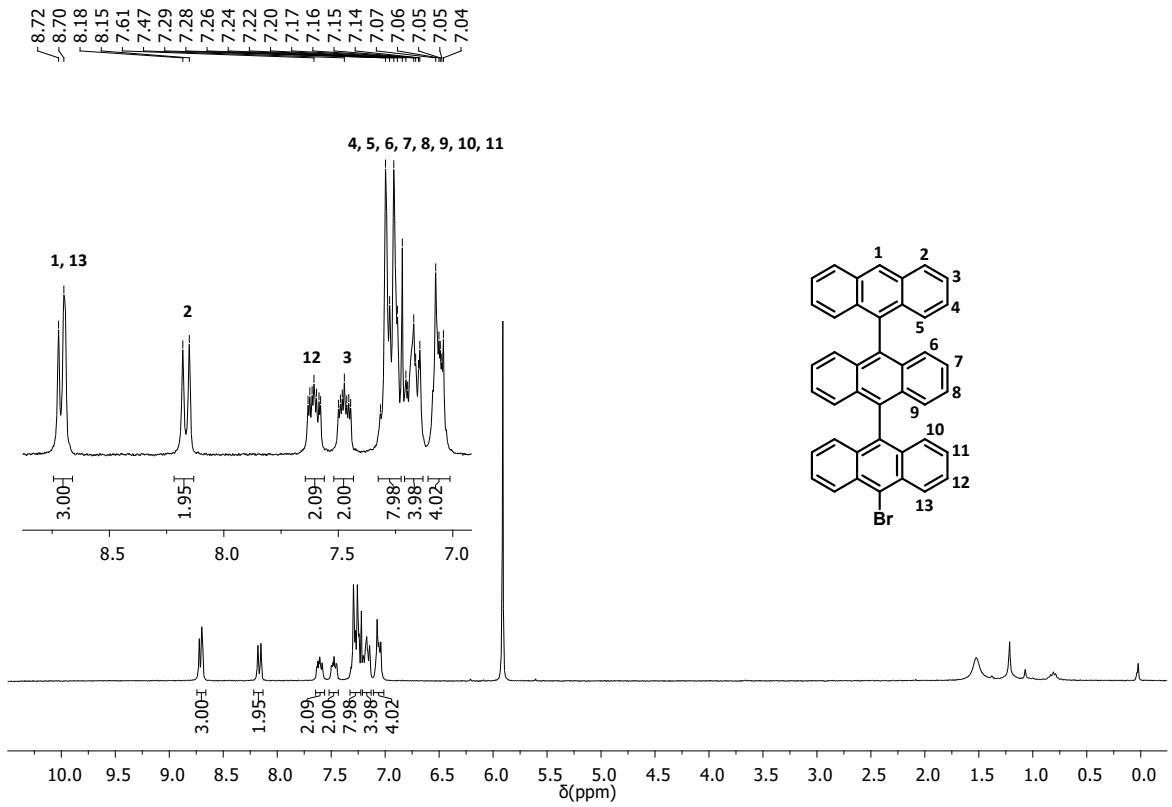

Figure S3a: ^{1}H-NMR spectrum of **1** dissolved in tetrachloroethane-d_2, 300 MHz, 333 K.

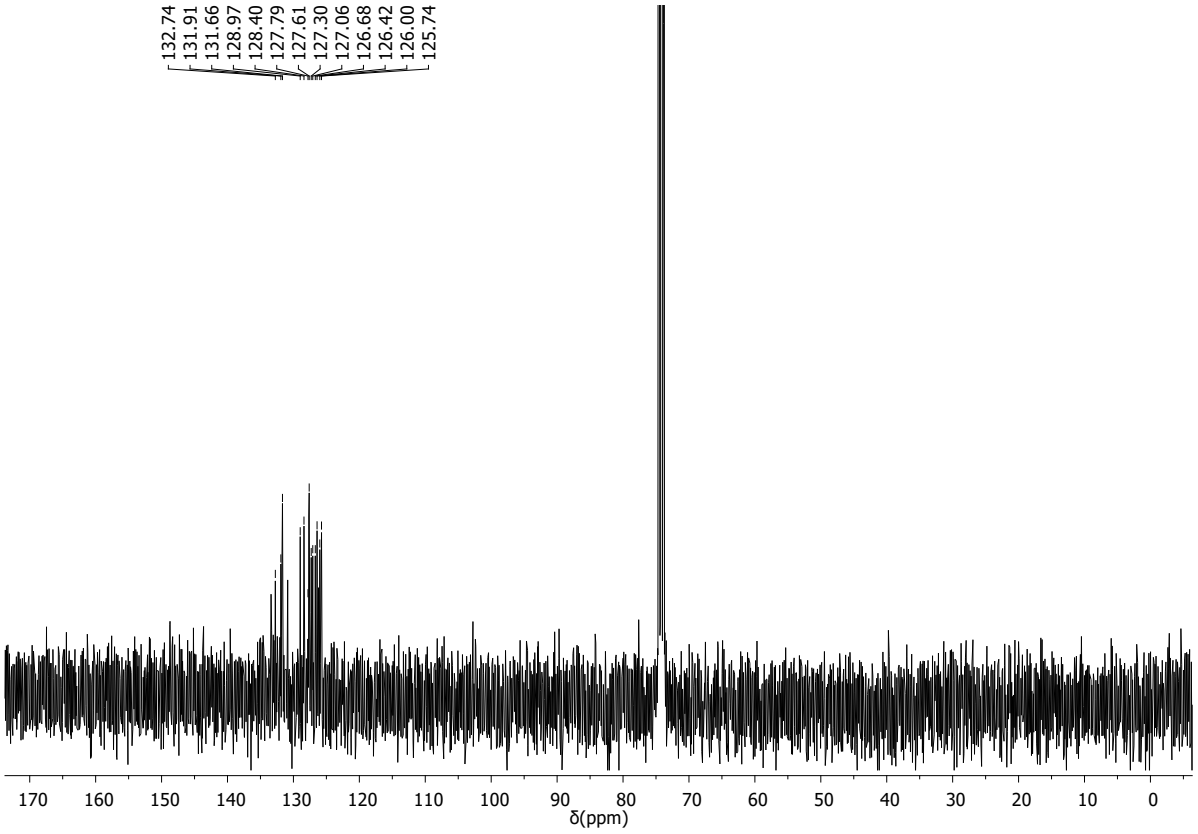

Figure S3b: ^{13}C-NMR spectrum of **1** dissolved in tetrachloroethane-d_2, 75 MHz, 333 K.

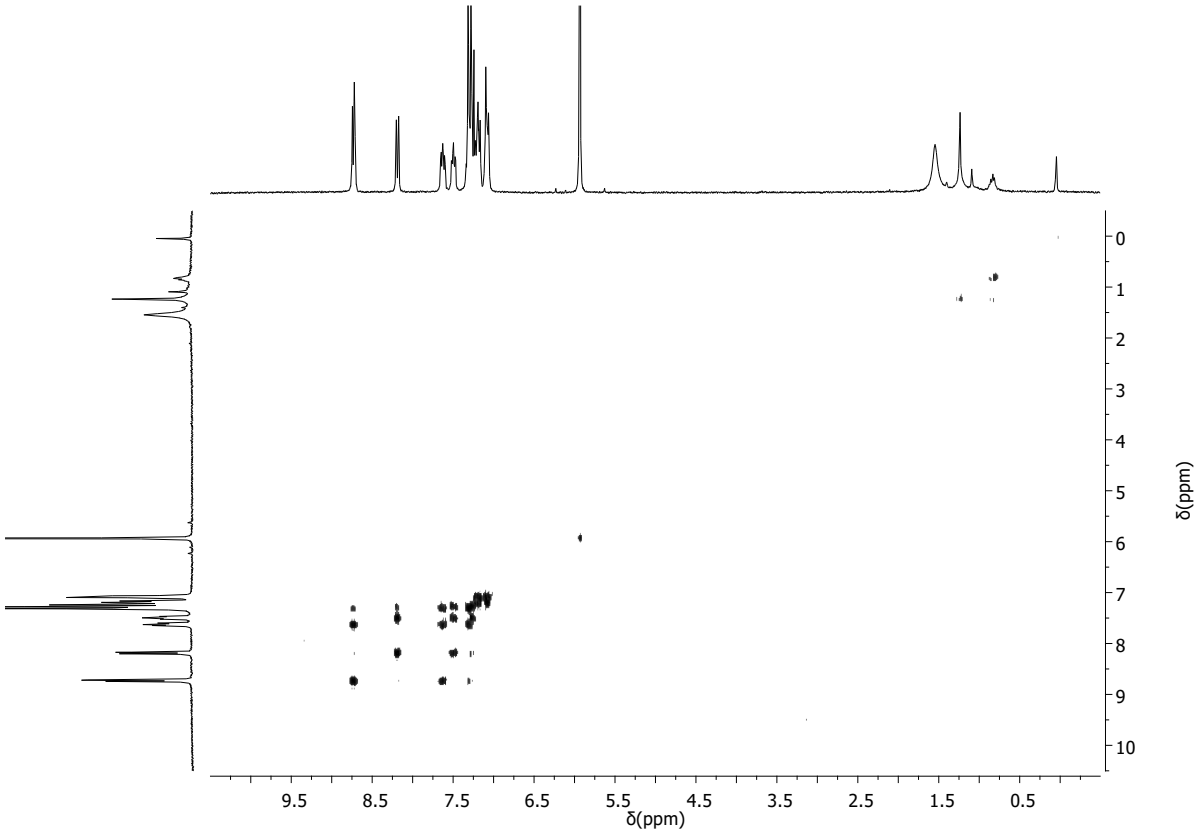

Figure S3c: ^{1}H/^{1}H-COSY-NMR spectrum of **1** dissolved in tetrachloroethane-d_2, 300 MHz, 333 K.

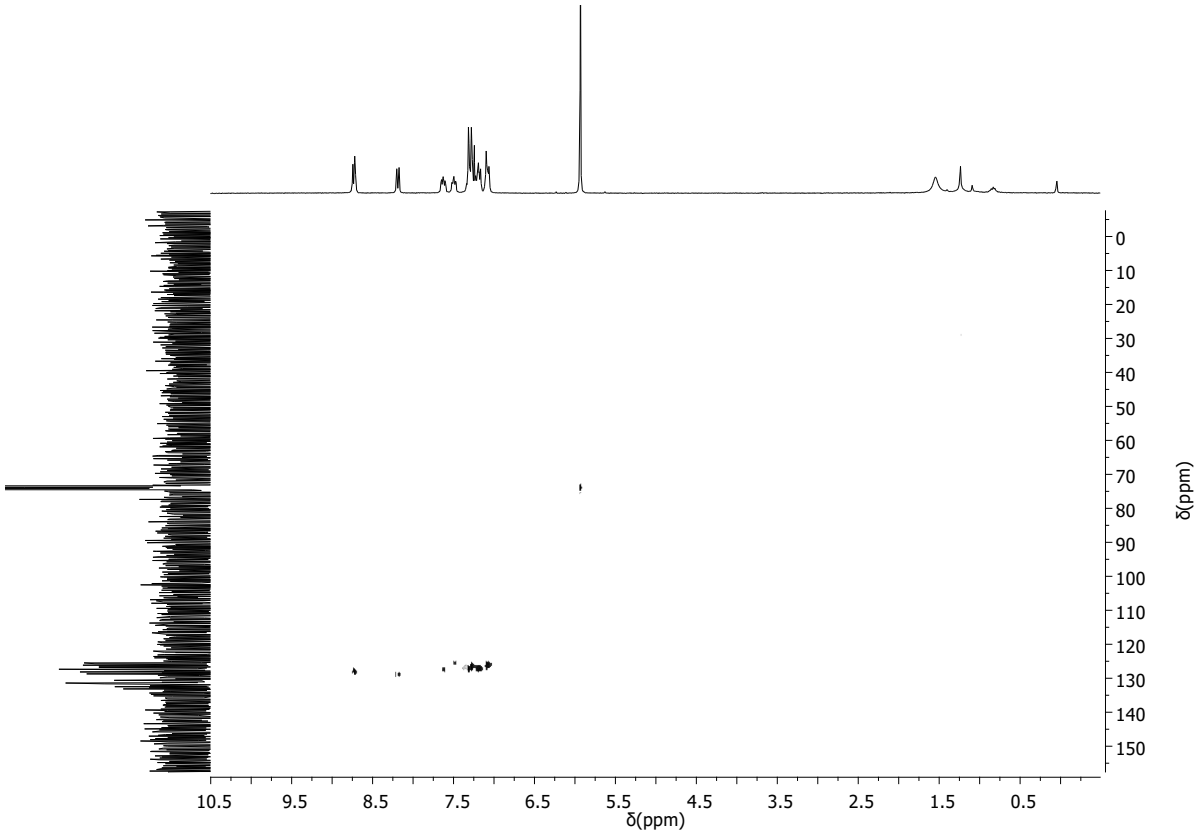

Figure S3d: HSQC-NMR spectrum of **1** dissolved in tetrachloroethane-d_2, 75 MHz, 333 K.

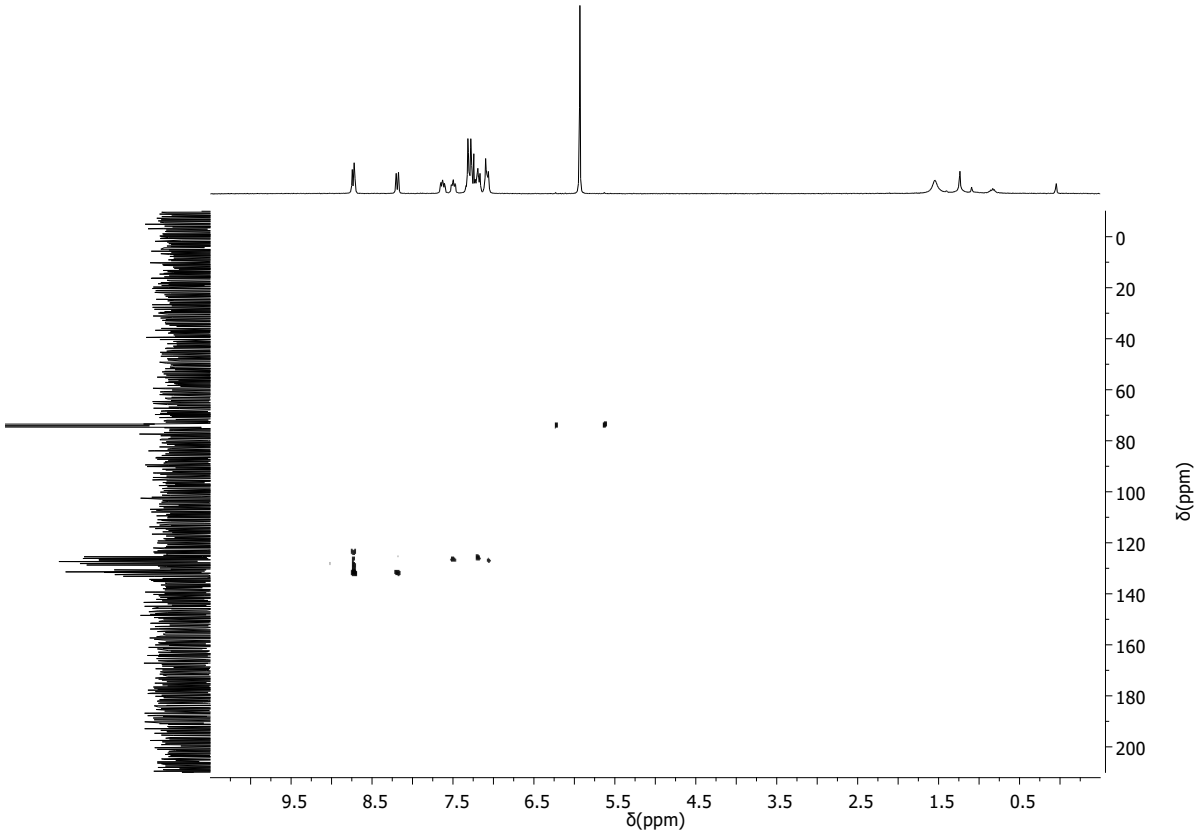

Figure S3e: HMBC-NMR spectrum of **1** dissolved in tetrachloroethane-d_2, 75 MHz, 333 K.

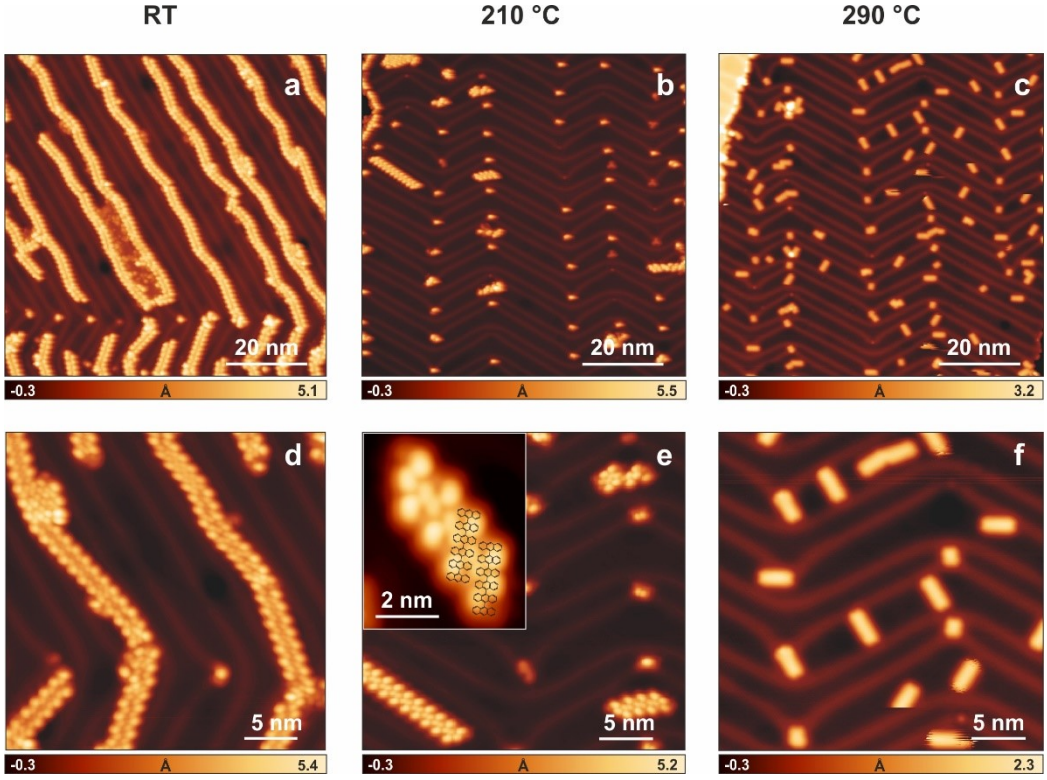

Figure S4. STM images of the Au(111) surface after deposition of precursor **1** at room temperature (RT), followed by successive annealing steps at the given temperatures (a-f). Inset (e): magnified STM image with superimposed chemical structures of the dimers after dehalogenative aryl-aryl coupling of **1** on the surface. Scanning parameters: a) $V = -1.0$ V, $I = 30$ pA, b) $V = -1.0$ V, $I = 30$ pA, c) $V = -1.0$ V, $I = 20$ pA, d) $V = -0.5$ V, $I = 30$ pA, e) $V = -0.3$ V, $I = 30$ pA, f) $V = -1$ V, $I = 20$ pA.

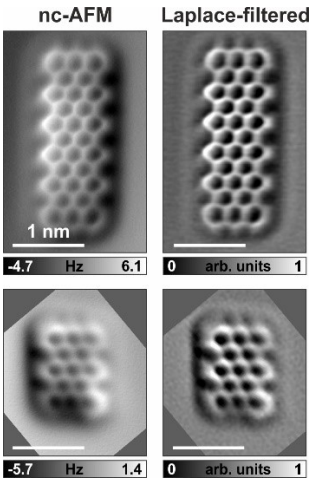

Figure S5. Left panels: nc-AFM frequency-shift images of **HA** (upper panel) and **TA** (lower panel). Scanning parameters: (top) tip height offset $\Delta z = 195$ pm above the STM setpoint $V = -5$ mV, $I = 100$ pA, (bottom) $\Delta z = 190$ pm above the STM setpoint $V = -5$ mV, $I = 100$ pA. Right panels: Corresponding Laplace-filtered versions of the left panels (also shown in Fig. 1).

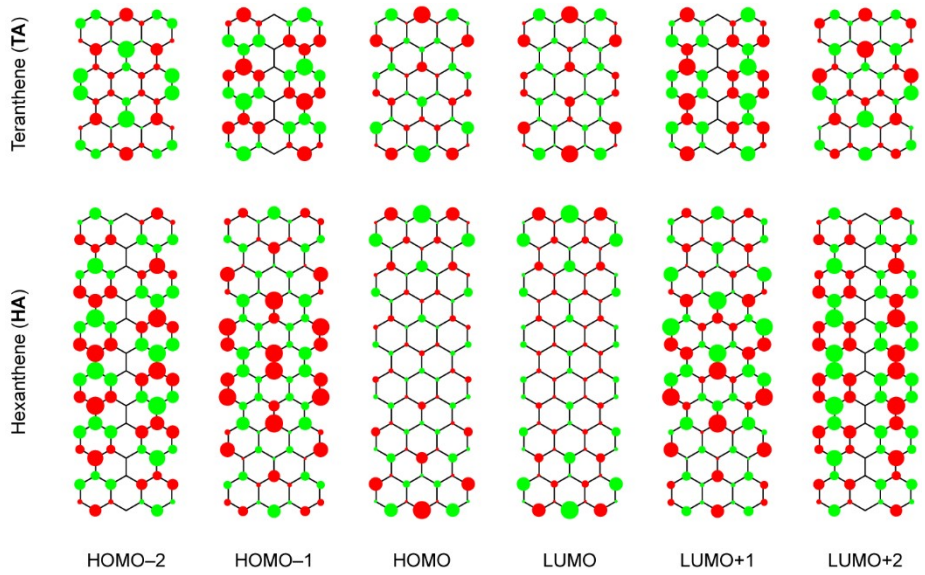

Figure S6. TB wave functions of HOMO–2 to LUMO+2 of **TA** (top) and **HA** (bottom). Size of the filled circles denotes amplitude of the wave function, while the two colors denote opposite phases of the wave function.

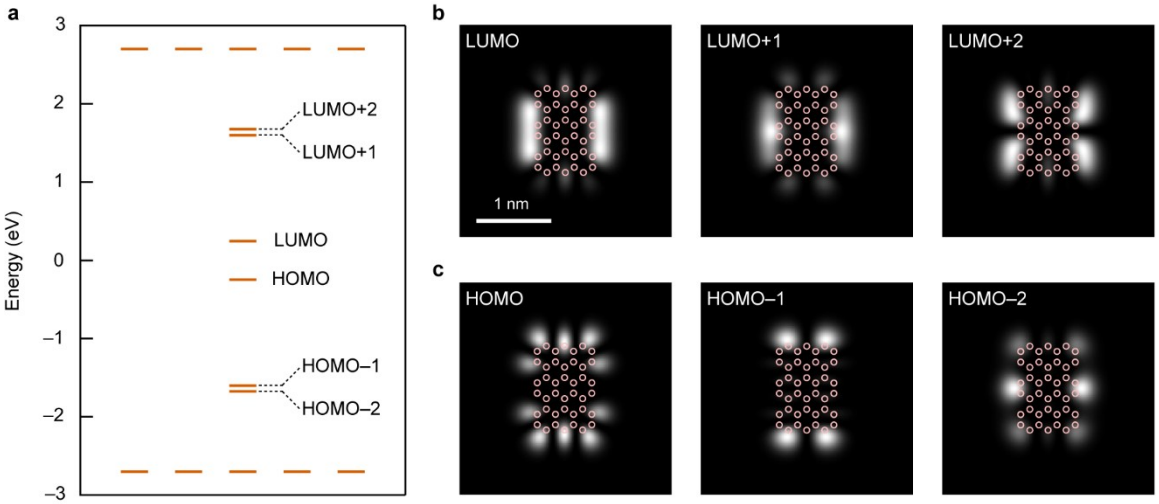

Figure S7. TB calculations on **TA**. (a) Gas phase TB energy spectrum of **TA** between ±3 eV. HOMO–2 to LUMO+2 states are labeled. The calculated frontier gap of **TA** is ~0.5 eV at nearest-neighbor TB level of theory. (b, c) TB-LDOS maps of the labeled states in (a) for the unoccupied (b) and occupied (c) channels. The carbon backbone of **TA** (colored circles) is superimposed as a guide to the eye. The maps are calculated at a height of 7 Å above the molecular plane.

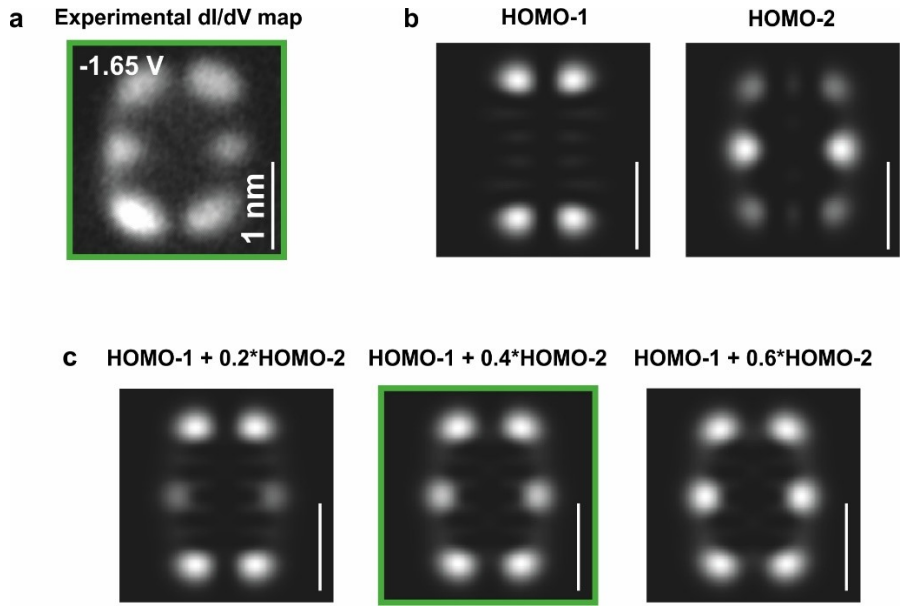

Figure S8. Intermixing of HOMO-1 and HOMO-2 states of **TA**. (a) *dI*/*dV* map of the resonance at –1.65 V. (b) TB-LDOS maps of the HOMO–1 and HOMO–2 of **TA**. The d*I*/d*V* map at –1.65 V contains features that are characteristic of both orbitals – that is, strong LDOS features at the termini (characteristic of HOMO–1, and to some extent, also HOMO–2) and slightly weaker LDOS features at the center of the armchair edges (characteristic of HOMO–2 exclusively). As shown in (c), mixing of the HOMO–2 LDOS (with a weight of 0.4) into the HOMO–1 LDOS clearly reproduces our experimental observation. The TB-LDOS maps are calculated at a height of 7 Å above the molecular plane.

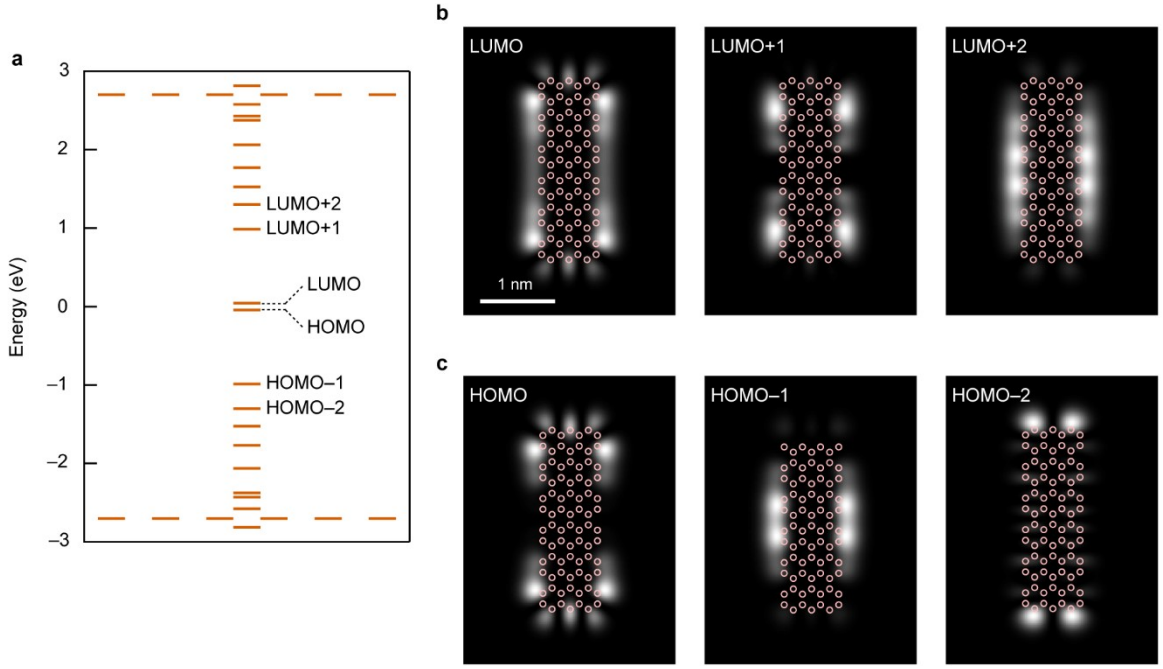

Figure S9. TB calculations on **HA**. (a) Gas phase TB energy spectrum of **HA** between ±3 eV. HOMO–2 to LUMO+2 states are labeled. The calculated frontier gap of **HA** is ~90 meV at nearest-neighbor TB level of theory, much less than that of **TA** at the same level of theory (Fig.

S7). (b, c) TB-LDOS maps of the labeled states in (a) for the unoccupied (b) and occupied (c) channels. The carbon backbone of **HA** (colored circles) is superimposed as a guide to the eye. The maps are calculated at a height of 7 Å above the molecular plane.

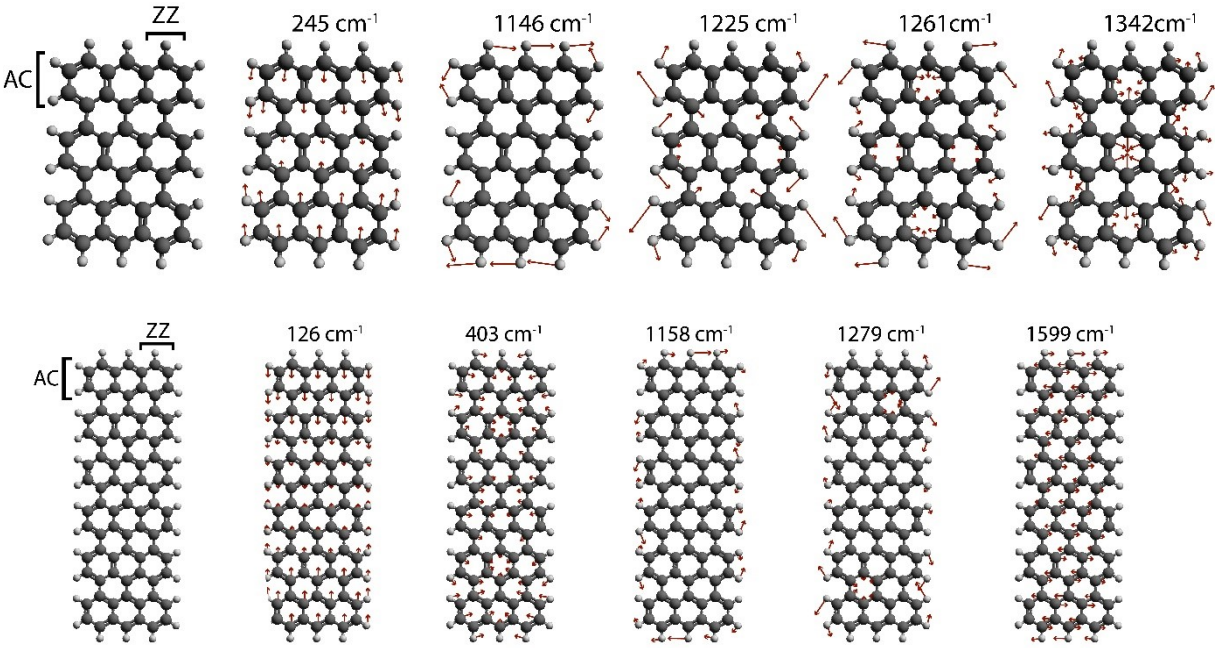

Figure S10: Raman normal mode analysis of teranthene (**TA**) (upper panel) and hexanthene (**HA**) (lower panel). Red arrows indicate amplitude and direction of atomic displacements.

- Modes at 245 and 126 cm^{-1}: longitudinal compressive mode (LCM)
- Mode at 403 cm^{-1}: radial breathing-like mode (RBLM)
- Modes at 1146 and 1158 cm^{-1}: CH-bending of zigzag edges
- Modes at 1225, 1261 and 1279 cm^{-1}: CH-bending armchair edges
- Mode at 1342 cm^{-1}: D mode
- Mode at 1599: G mode

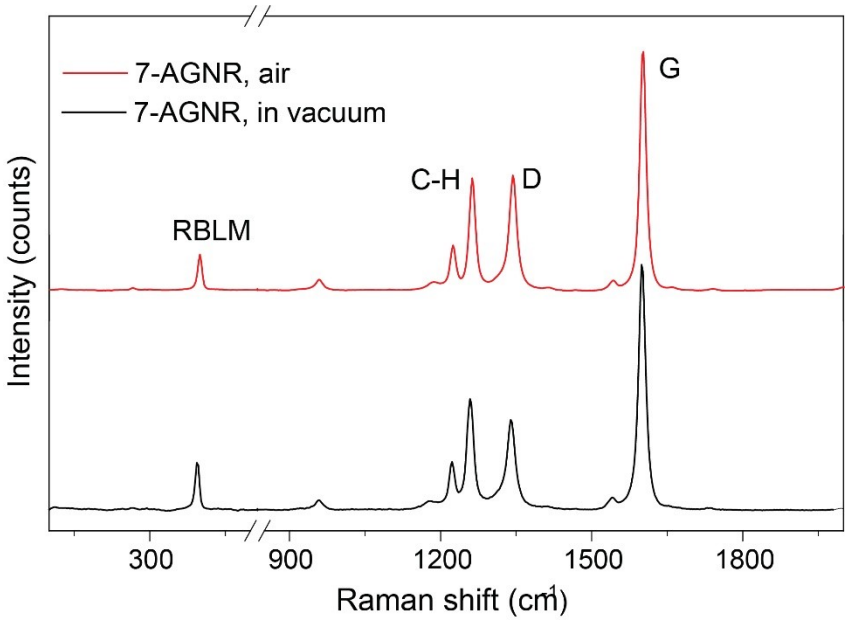

Figure S11. Raman spectroscopy of long 7-AGNRs in ultra-high vacuum (in black) and in air (in red) measured with 532 nm laser energy.

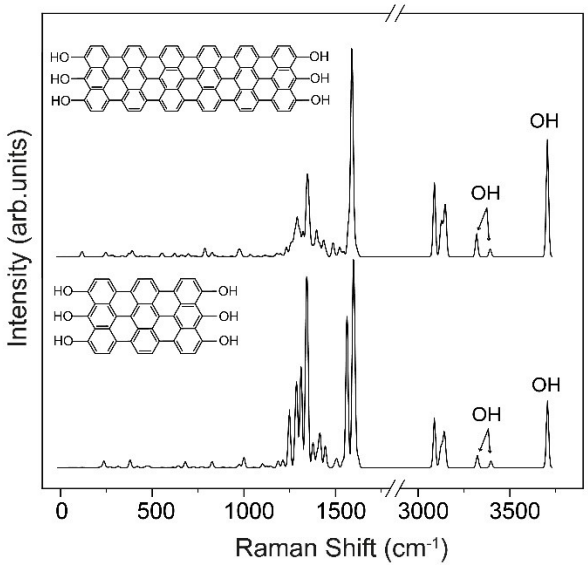

Figure S12. Simulated Raman spectra of HA and TA with OH-terminated zigzag edges.